CDDpress

www.nature.com/cddis

ARTICLE OPEN

Tumor microenvironment-induced FOXM1 regulates ovarian cancer stemness

Chiara Battistini[1], Hilary A. Kenny[2], Melissa Zambuto[1], Valentina Nieddu[1], Valentina Melocchi[3], Alessandra Decio[4], Pietro Lo Riso[5], Carlo Emanuele Villa[6], Alessia Gatto[1], Mariacristina Ghioni[7], Francesca M. Porta[7,8], Giuseppe Testa[5,9], Raffaella Giavazzi[4], Nicoletta Colombo[10,11], Fabrizio Bianchi[3], Ernst Lengyel[2] and Ugo Cavallaro[1]✉

In ovarian tumors, the omental microenvironment profoundly influences the behavior of cancer cells and sustains the acquisition of stem-like traits, with major impacts on tumor aggressiveness and relapse. Here, we leverage a patient-derived platform of organotypic cultures to study the crosstalk between the tumor microenvironment and ovarian cancer stem cells. We discovered that the pro-tumorigenic transcription factor FOXM1 is specifically induced by the microenvironment in ovarian cancer stem cells, through activation of FAK/YAP signaling. The microenvironment-induced FOXM1 sustains stemness, and its inactivation reduces cancer stem cells survival in the omental niche and enhances their response to the PARP inhibitor Olaparib. By unveiling the novel role of FOXM1 in ovarian cancer stemness, our findings highlight patient-derived organotypic co-cultures as a powerful tool to capture clinically relevant mechanisms of the microenvironment/cancer stem cells crosstalk, contributing to the identification of tumor vulnerabilities.

Cell Death and Disease (2024)15:370 ; https://doi.org/10.1038/s41419-024-06767-7

INTRODUCTION

Epithelial ovarian cancer (OC) is the most lethal gynecological cancer worldwide [1], and high-grade serous OC (HGSOC) is its most frequent and aggressive subtype, with a survival rate of only 30% at 5 years [2]. HGSOC is often diagnosed at an advanced stage, when the disease has already spread into the peritoneal cavity [3]. Moreover, despite an initial response to first-line treatments, 70% of HGSOC relapse within 2 years [1], and almost all recurrent HGSOC ultimately develop chemoresistance and become unresponsive to standard treatments [4].

Among the factors implicated in the aggressiveness of HGSOC, a role has been attributed to a small subpopulation of cells named ovarian cancer stem cells (OCSC). These cells have the ability to self-renew and to initiate tumorigenesis, therefore they are crucially involved in the process of peritoneal dissemination and colonization; moreover, they are intrinsically resistant to cytotoxic treatments, thereby evading standard chemotherapy and fueling tumor re-growth and relapse [4]. These features make OCSC an optimal therapeutic target to tackle OC, but to reach this goal there is an urgent need to gain further insights into OCSC biology. In this context, the tumor microenvironment (TME) has been implicated in OC stemness, thus promoting the acquisition of an aggressive phenotype [5]. Moreover, previous studies have demonstrated that the TME impacts significantly the response of OC cells to chemotherapy [6]. Therefore, it is fundamental to generate preclinical in vitro models that incorporate the TME, to better mimic the OC biology and predict more faithfully its response to therapies, and, importantly, to address the specific mechanisms of its crosstalk with OCSC.

The peritoneal surface is the preferential site of HGSOC dissemination and offers an optimal niche to metastasizing cells [7]. To recapitulate this process in vitro, three-dimensional multicellular organotypic models have been established using human omental fibroblasts and mesothelial cells. Adding OC cells to organotypic co-cultures has allowed to elucidate some of the molecular mechanisms that govern the OC/TME crosstalk [8–11]. However, these studies have relied on established OC cell lines, which have an intrinsically limited disease relevance. Furthermore, while the organotypic setting offers an optimal tool to explore the influence of peritoneal TME on OC stemness-related features, so far it has not been applied to this objective.

In the current study, we report the discovery of FOXM1 as a major effector of the TME/OCSC interplay. FOXM1 is a transcription factor belonging to the conserved forkhead box (FOX) family, which has been associated with poor prognosis in several cancer types. The TCGA molecular profiling of OC reported altered FOXM1 signaling in 84% of cases [12], in agreement with the functional contribution of the transcription factor to various

[1]Unit of Gynaecological Oncology Research, European Institute of Oncology IRCCS, 20139 Milan, Italy. [2]Department of Obstetrics and Gynecology, Section of Gynecologic Oncology, University of Chicago, Chicago, IL 60637, USA. [3]Cancer Biomarkers Unit, Fondazione IRCCS Casa Sollievo della Sofferenza, 71013 San Giovanni Rotondo, FG, Italy. [4]Laboratory of Cancer Metastasis Therapeutics, Mario Negri Institute for Pharmacological Research - IRCCS, 20156 Milan, Italy. [5]Department of Experimental Oncology, European Institute of Oncology IRCSS, Milan, Italy. [6]Human Technopole, Viale Rita Levi-Montalcini 1, 20157 Milan, Italy. [7]Division of Pathology, European Institute of Oncology IRCCS, 20141 Milan, Italy. [8]School of Pathology, University of Milan, 20122 Milan, Italy. [9]Department of Oncology and Hemato-Oncology, University of Milan, Milan, Italy. [10]Division of Gynecologic Oncology, European Institute of Oncology IRCCS, 20141 Milan, Italy. [11]University of Milan-Bicocca, 20126 Milan, Italy. ✉email: ugo.cavallaro@ieo.it

Edited by Gerry Melino

Received: 9 April 2024 Revised: 16 May 2024 Accepted: 21 May 2024
Published online: 28 May 2024

aspects of OC malignancy [13]. Yet, whether FOXM1 is involved in OC stemness and in the pathophysiology of OCSC has remained elusive.

Here, we built on a platform of clinically relevant patient-derived organotypic co-cultures to shed light on the crosstalk between OCSC and their TME. Notably, the TME-mediated induction of FOXM1 in OCSC is crucial for their survival in the omental niche, but also a vulnerability that, if successfully targeted, may improve the response of tumor cells to drug treatments.

RESULTS

Contact with TME induces transcriptional reprogramming in bulk OC cells and OCSC

To investigate the crosstalk between OC cells and their microenvironment in a clinically relevant setting, we reconstructed in vitro a 3D organotypic model of ovarian TME, entirely composed of patient-derived primary cells. We used tumor cells derived from ascites of HGSOC patients, cultured either as bulk, adherent population or as clonal spheres under non-adherent conditions. This method exploits fundamental properties of CSC, namely their ability to resist *anoikis*, to self-renew, and to proliferate when seeded at low density in non-adherent conditions, to enrich primary tumor cultures for cells endowed with stem-like features [4]. The peritoneal microenvironment was recapitulated by the co-culture of primary mesothelial cells and fibroblasts derived from human omental biopsies [14] (Supplementary Fig. 1A, B). Single-cell suspensions of primary OC cells, cultured either as adherent cells (referred to as "bulk") or as OCSC-enriched spheres, were labeled with CMFDA (a green fluorescent dye) and then seeded on top of omental stromal cells, to generate 3D organotypic cultures of ovarian TME (Fig. 1A and Supplementary Fig. 1C).

After 48 h, 3D co-cultures were dissociated to single cells and CMFDA-labeled HGSOC cells were isolated by FACS and subjected to RNA-seq. Six independent 3D organotypic co-cultures (i.e., from six different patients, Supplementary Table S1) were analyzed and tumor cells from the co-cultures were compared to cells cultured without TME. Peritoneal TME induced a dramatic transcriptional reprogramming in HGSOC cells, with 1494 differentially expressed genes (DEGs) in bulk cancer cells and 2771 DEGs in OCSC (Fig. 1B and Supplementary Tables S2 and S3). A large fraction of DEGs were specific to either bulk OC or OCSC (Fig. 1C; $p < 0.001$, hypergeometric test), indicating that the TME induced different transcriptional responses in the two cell subpopulations. Interestingly, Ingenuity Pathway Analysis (IPA) showed that the top regulated pathways in DEGs specific to bulk OC were mainly related to cytoskeletal remodeling, Rho-mediated motility, and metabolic processes such as oxidative phosphorylation (Fig. 1D). In contrast, pathways up-regulated in OCSC when co-cultured with the TME related to cell cycle regulation, S-phase entry and chromosomal replication (Fig. 1E).

These data demonstrated that TME exerted a distinct transcriptional program in primary OC cells and OCSC, yet with a remarkably divergent response in the two cell populations.

TME induces FOXM1 specifically in OCSC

We performed an Upstream Regulator Analysis on the RNA-seq dataset described above to identify molecular hubs regulated by peritoneal TME in OCSC. One of the most prominent transcriptional regulators activated upon contact with the TME was FOXM1 (z-score = 5.088; p-value = $2.61*10^{-20}$; Fig. 1F; Supplementary Table S4), a major driver of proliferation, survival and tumorigenesis [15]. Gene Set Enrichment Analysis (GSEA) indeed showed a significant enrichment of the FOXM1 pathway in OCSC when cultured on TME (NES = +2.29; q-value < 0.001) Supplementary Fig. 2A). A qPCR analysis for FOXM1 expression confirmed the TME-induced activation of FOXM1 (Fig. 1G). Moreover, a set of cell cycle-related FOXM1 target genes (*AURKA*, *CCNB1*, *CDK1*, and *PLK1*) was also induced in OCSC cultured on TME (Fig. 1G). Notably, immunofluorescence staining showed the presence of FOXM1 in the nuclei of primary, HGSOC-derived OCSC cultured on TME, and not in the same OCSC in the absence of TME (Supplementary Fig. 2B).

In order to further investigate the characteristics of FOXM1-expressing OCSC cells, we performed a scRNAseq on two of the six primary samples profiled by global RNAseq (namely OC1 and OC4), after a 48-h culture on TME as bulk cells or as OCSC. Bulk OC cells and OCSC clustered in two separated areas of the UMAP (Fig. 2A, left), in line with their diverse response to co-culture with TME as observed with global RNAseq. Moreover, when the cell cycle phase for each cell was inferred from the transcriptome (G1, S, G2M), we observed that cycling cells were much more represented among OCSC than in bulk cells (Fig. 2A, middle), and FOXM1 expression was markedly higher in these cycling cells (Fig. 2A, right). FOXM1 was also more frequently expressed and at consistently higher level in OCSC compared to bulk cells in both primary samples (Supplementary Fig. 2C) and in all the phases of cell cycle (Fig. 2B). Moreover, we mapped on the UMAP the expression levels of the cell cycle-related FOXM1 target genes (*AURKA*, *CCNB1*, *CDK1*, and *PLK1*) previously analyzed by qPCR (Fig. 1G), and we observed their co-localization with cycling cells expressing FOXM1 (Fig. 2C). Overall, these data revealed at a single-cell level that FOXM1 is specifically induced by TME in OCSC, and it is closely related to cell cycle progression.

Finally, when we interrogated by GSEA a large cohort of HGSOC patients, i.e. the TCGA-OC dataset ($N = 535$; see methods), we observed the enrichment for pathways related to cell cycle progression in high-FOXM1 compared to low-FOXM1 tumors (Supplementary Fig. 3), in line with the effect of TME on OCSC. This supported the ability of our organotypic model to recapitulate clinically relevant, FOXM1-mediated traits of the disease.

FOXM1 is required for OC stemness

The role of FOXM1 in OC stemness has been studied only in cell lines and with limited mechanistic insights [16–18]. Thus, we initially explored the functional contribution of FOXM1 to stemness in clinically relevant models using primary HGSOC cultures and blocking FOXM1 function with Thiostrepton, a natural cyclic oligopeptide antibiotic that is widely used as a FOXM1 inhibitor [19]. Thiostrepton had no significant effect on the viability of bulk, adherent OC cells (Fig. 3A and Supplementary Fig. 4A), while it efficiently inhibited sphere formation (Fig. 3B and Supplementary Fig. 4B), suggesting the specific involvement of FOXM1 in promoting stem-like properties.

To gain further insights into the role of FOXM1 in OC stemness, we sought to identify an experimental model suitable for genetic manipulation, which mirrored the behavior of primary OCSC cultured on TME. Sphere cultures were generated from a panel of OC cell lines and were analyzed for *FOXM1* expression in OCSC cultured with or without peritoneal TME. In contrast with the consistent and reproducible behavior of several primary OC samples in the organotypic co-cultures, only the TYK-nu cells exhibited a strong TME-induced upregulation of FOXM1 among the cell lines tested (Supplementary Fig. 4C). While this somehow confirmed the limited potential of various classical OC lines to recapitulate certain aspects of the human disease [20, 21], it pointed to TYK-nu cells as a suitable system for a loss-of-function approach. Lentiviral-mediated shRNA transduction was applied to assess the impact of ablating FOXM1 (Supplementary Fig. 4D) on stem-related traits both in vitro and in vivo. As shown in Fig. 3C, the knockdown of FOXM1 reduced the ability of TYK-nu cells to form spheres, while no major effect were observed on their proliferation in adherent conditions (Supplementary Fig. 4E).

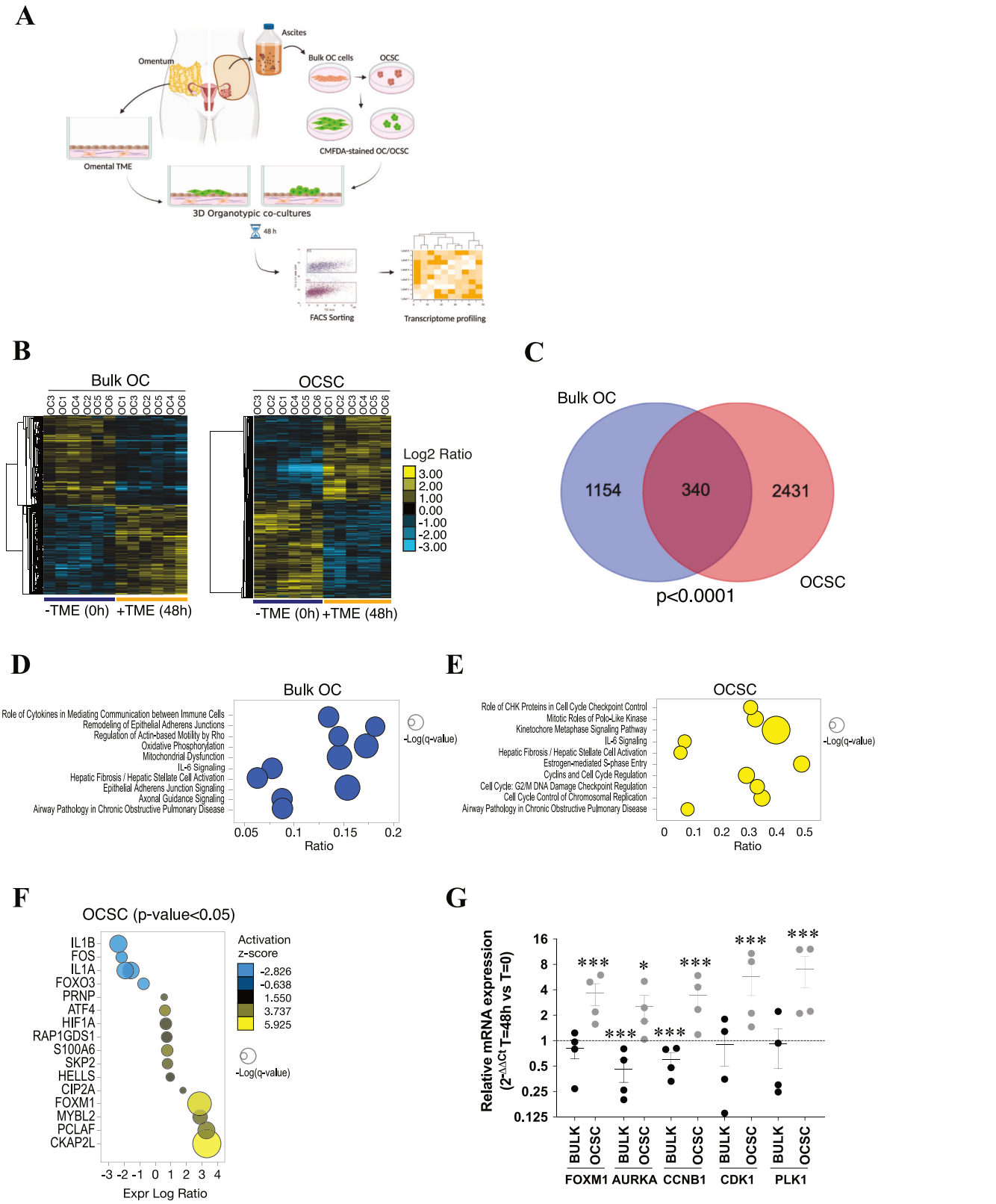

Tumor initiation is a key defining property of CSC; we therefore tested the effect of FOXM1 ablation on the tumor-initiating ability of OC cells. To this aim, an in vivo extreme limiting dilution assay (ELDA) [22] was performed with TYK-nu cells knocked down for FOXM1 expression vs control cells. Nude mice were injected subcutaneously with a decreasing number of cells (from $5*10^6$ to $1*10^4$ cells/mouse) and monitored for tumor formation. ELDA calculation was based on the number of mice with palpable tumors at 21 days after the injection (Supplementary Fig. 4F), which revealed that FOXM1 knockdown

Fig. 1 The TME induces transcriptional reprogramming in bulk OC cells and OCSC and activates FOXM1 pathway in OCSC. A Schematic representation of the patient-derived organotypic model. CMFDA-labeled bulk OC cells and OCSC are FACS-isolated after 48 h of co-culture with TME (fibroblasts and mesothelial cells) and subjected to RNA sequencing. Created with BioRender.com. **B** Hierarchical clustering analysis of differentially expressed genes in bulk OC and OCSC of 6 HGSOC samples (OC1-6) with or without the interaction with tumor microenvironment (TME). The heatmap shows gene expression change (log_2 ratios) as per the legend. **C** Venn diagrams showing the number of DEGs regulated by TME in bulk OC and OCSC (hypergeometric test $p = 2.377e{-}19$). DEGs are listed in Supplementary Tables S2 and S3. Bubble plots showing results of the Canonical Pathways Analysis of Ingenuity Pathways Analysis (IPA) in bulk OC (**D**) and OCSC (**E**). Bubble size represents the inverse of Logarithmic (-Log) of significance (q-value); for each pathway, ratio is the number of genes in our list over the total number of genes in the specific pathway. Only pathways with q-value ≤ 0.05 are shown. **F** Bubble plot showing the results of Upstream Regulator Analysis of IPA. Upstream modulators are predicted to be modulated by contact with TME in OCSC and are listed in Supplementary Table S4. Bubble size is proportional to inverse of Logarithmic (-Log) of significance [e.g., -Log(p-value), p-value < 0.05; Student's t test] of z-score. Bubble colors refer to activation z-score, as per the legend. Only modulators with coherent expression trend with the activation z-score are shown. **G** mRNA expression of *FOXM1* and its target genes (*AURKA*, Aurora Kinase A, *CCNB1*, Cyclin B1, *CDK1*, Cyclin-dependent Kinase 1, *PLK1*, Polo-like Kinase 1) was analyzed by qRT-PCR in 4 of the 6 patients profiled in panel B (OC1-4). Data are represented as a relative mRNA expression ($2^{-\Delta\Delta Ct}$) of bulk OC cells (in black) and OCSC (in gray) co-cultured with TME for 48 h (T = 48 h) compared to cells grown in the absence of TME (T = 0, dashed line). The dots represent each gene's relative mRNA expression in each sample, while bars and whiskers represent its mean ± SEM among the 4 samples analyzed. Comparisons between experimental groups were done with two-sided Student's t test; *$p < 0.05$, ***$p < 0.005$.

reduced the frequency of tumor-initiating cells by 4.6 times (Fig. 3D).

Overall, these data demonstrated that FOXM1 is required to sustain stem-like traits and tumor initiation capacity in OC cells.

TME-dependent induction of FOXM1 is mediated by FAK/YAP signaling

In an attempt to elucidate the molecular mechanisms that underlie FOXM1 induction by TME in OCSC, we first tested the possible involvement of soluble factors. This, however, appeared not to be the case since treatment of OCSC with TME-derived conditioned medium did not induce FOXM1 expression (Supplementary Fig. 5A). We then focused on integrin signaling, a pathway stimulated by intercellular contact as well as adhesion to extracellular matrix (ECM) [23], which is known to induce FOXM1 expression [24]. To test this possibility in our system, we seeded sphere-derived cells from TYK-nu and from primary OC samples on different ECM, such as collagen or fibronectin, and we observed a strong transcriptional induction of FOXM1 (Supplementary Fig. 5B, C). Based on the notion that Focal Adhesion Kinase (FAK) is a classical effector of the integrin pathway [23], we investigated its potential involvement in TME-dependent upregulation of FOXM1. FAK was not active in TYK-nu and in primary OCSC when cultured alone as spheres, where also FOXM1 was not expressed (Fig. 4A). To visualize the status of FAK in sphere-derived cells cultured on the TME, we performed immunofluorescence staining for phospho-FAK in the organotypic setting. As shown in Fig. 4B, C, FAK was strongly activated in OCSC specifically upon co-culture with TME.

FAK is known to stimulate YAP signaling [25], and FOXM1 is a direct transcriptional target of YAP [26, 27]. Thus, YAP signaling could be activated by TME in OCSC downstream to FAK activation, resulting in FOXM1 upregulation. In support of this hypothesis, GSEA showed significant enrichment for YAP signature not only in OCSC upon co-culture with TME but also in high-FOXM1 vs. low-FOXM1 samples in the TCGA-OC dataset (Supplementary Fig. 5D). On this basis, we investigated the role of the FAK/YAP axis in the regulation of FOXM1. OCSC from TYK-nu and from primary HGSOC cells were cultured on TME in the presence of the YAP inhibitor Verteporfin or the FAK inhibitor Defactinib. Both compounds reduced the TME-mediated induction of FOXM1 (Fig. 4D, E and Supplementary Fig. 5E, F). These data implicated both FAK and YAP in FOXM1 regulation in the OCSC/TME co-culture setting. We could then demonstrate that, on one hand, TYK-nu cells treated with Defactinib displayed a reduction in YAP nuclear localization (Supplementary Fig. 5G) and, on the other, Defactinib significantly reduced YAP nuclear localization in TYK-nu OCSC cultured on TME (Fig. 4F, G). Thus, in our cellular model FAK and YAP act in the same axis.

Taken together, this set of data describes a novel cascade whereby peritoneal TME induces the activation of a FAK-YAP axis in OCSC that ultimately leads to FOXM1 induction

Interfering with FOXM1 pathway impairs the survival of OCSC on TME and synergizes with PARP inhibitors

The TME-induced FOXM1 activation may represent a specific vulnerability of OCSC and, therefore, interfering with this process could unveil a promising stem cell-eradicating approach. To verify this hypothesis, we first tested if the pharmacological inhibition or genetic downmodulation of FOXM1 could affect TME-mediated activation of its downstream pathway. The expression of *FOXM1* itself and of its classical target genes (i.e., *AURKA*, *CCNB1*, *CDK1*, *PLK1*) upon co-culture with TME was analyzed in primary OCSC from OC1 patient in the presence or absence of Thiostrepton, as well as in FOXM1-knockdown vs control OCSC from TYK-nu cells. Both FOXM1 inhibition (Fig. 5A) and its silencing (Fig. 5B) reduced significantly the TME-dependent upregulation of FOXM1 target genes. Moreover, primary OCSC re-isolated from co-cultures treated with Thiostrepton exhibited a significant decrease in sphere formation as compared to OCSC from untreated co-cultures (Fig. 5C). Overall, these data suggested that blocking the TME-mediated induction of FOXM1 might be a strategy to interfere with the stem-related properties of OCSC.

To explore such a possibility, we first generated TYK-nu cells stably tagged with red fluorescent protein (RFP), which were then cultured either as bulk, adherent cells or as OCSC on the TME for 6 days in the presence or absence of Thiostrepton. While Thiostrepton did not affect the survival of adherent cells, it significantly reduced the viability of OCSC (Fig. 6A, B). Analogous results were obtained in two different primary samples, with a specific effect of Thiostrepton on survival of OCSC (Fig. 6C, D). These data suggested that FOXM1 inhibition could target the stem cell compartment of HGSOC in the context of the omental niche.

Based on these results, we reasoned that the ability of FOXM1 inhibition to target OCSC would be particularly relevant in the maintenance therapy setting, which aims at preventing or delaying OCSC-driven tumor recurrence once the bulk of the tumor has been removed by surgery and cytotoxic treatments. Intriguingly, PARP inhibitors (PARPi) are commonly used as maintenance therapy in HGSOC patients with homologous recombination defects [28–30], and studies conducted in other cancer types suggested that FOXM1 inhibitors synergize with this class of drugs [31, 32], thanks to the reduced expression of homologous recombination-related genes which are among FOXM1 targets. On these premises, we investigated the effect of co-inhibiting PARP and FOXM1 in OCSC co-cultured with the TME. TYK-nu/RFP sphere-derived cells were treated for 6 days with

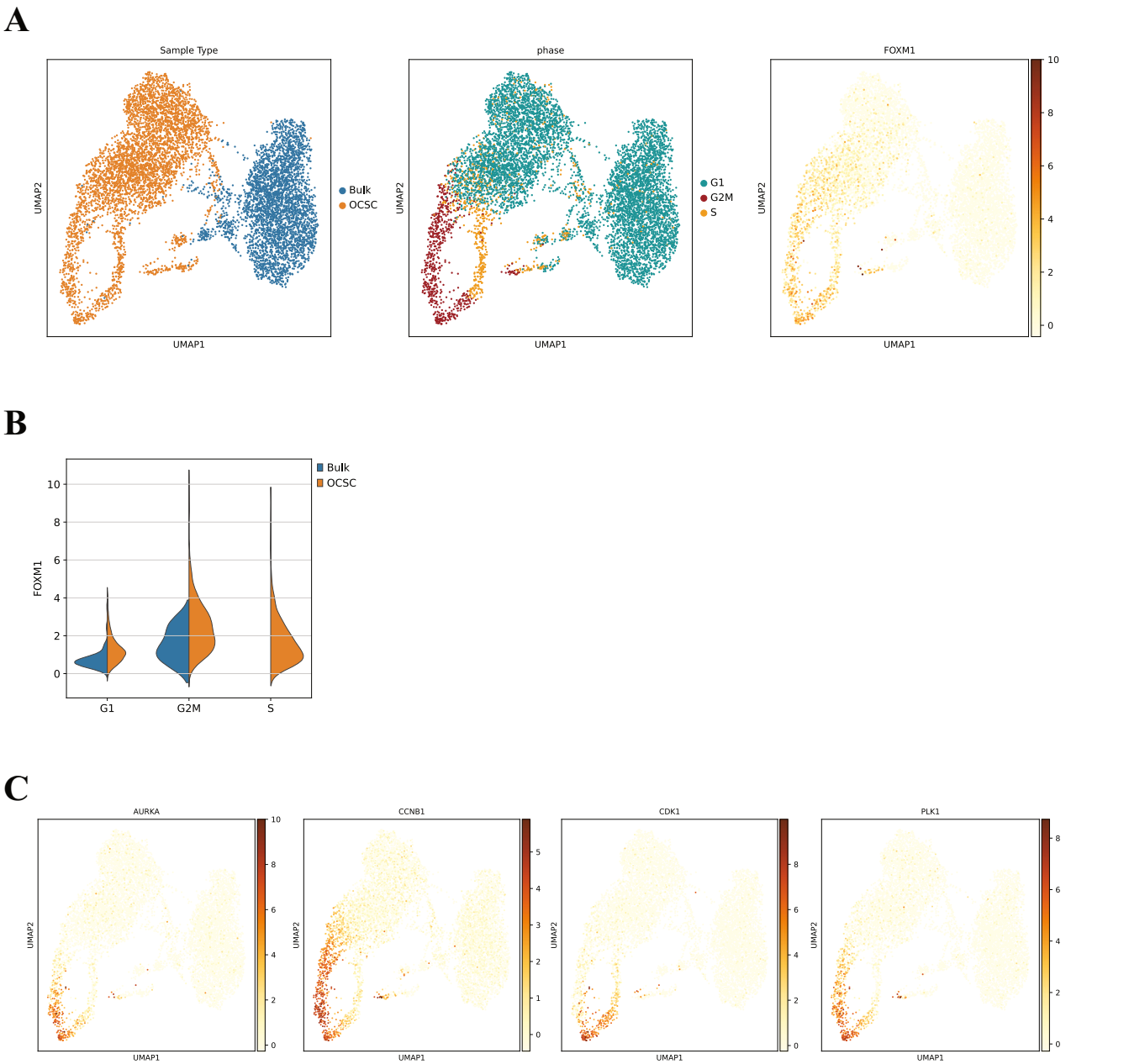

Fig. 2 Single cell transcriptomics reveal FOXM1 as an OCSC-specific gene closely related to cell cycle progression. A UMAP representation of single cell data, mapping either the sample type (left panel), inferred cell cycle phases (middle panel) and *FOXM1* expression (right panel). **B** Violin plot representing the level of expression of the *FOXM1* gene in FOXM1 positive cells in the considered sample types (bulk OC in blue and OCSC in orange) divided by cell cycle phases (x axis). **C** UMAP representation of single cell data, mapping the expression of cell cycle related genes (*AURKA*, Aurora Kinase A, *CCNB1*, Cyclin B1, *CDK1*, Cyclin-dependent Kinase 1, *PLK1*, Polo-like Kinase 1).

different doses of the PARPi Olaparib and Thiostrepton, alone or in combination. We observed a strong synergism between PARPi and FOXM1 inhibition in reducing the number of residual TYK-nu OCSC cultured on TME (Fig. 6E). To validate these findings in a more clinically relevant setting, we performed the same experiment on OCSC derived from two distinct HGSOC primary samples, and in both we observed an additive effect of the two drugs (Fig. 6F, G).

Overall, these data demonstrated that the TME-induced FOXM1 upregulation is a vulnerability of OCSC, and can render them more responsive to PARPi, thus suggesting that a combinatorial treatment in the maintenance setting could successfully delay, or even prevent, tumor recurrence.

DISCUSSION

The TME has long been known to influence the pathophysiology of tumor cells, affecting all phases of cancer progression as well as its responsiveness to treatments [6]. Particularly intriguing, in this regard, is the impact of TME on CSC: given the contribution of CSC to tumor initiation, dissemination, recurrence and drug resistance [4], dissecting the regulatory circuits that link the TME to their function may unveil vulnerabilities that could lead to tumor-eradicating therapies.

In the context of HGSOC, the peritoneum is the primary site of OCSC-driven dissemination and recurrence [33]. Thus, its crosstalk with OCSC is expected to play a central role in tumor malignancy and to have relevant clinical implications. To investigate the

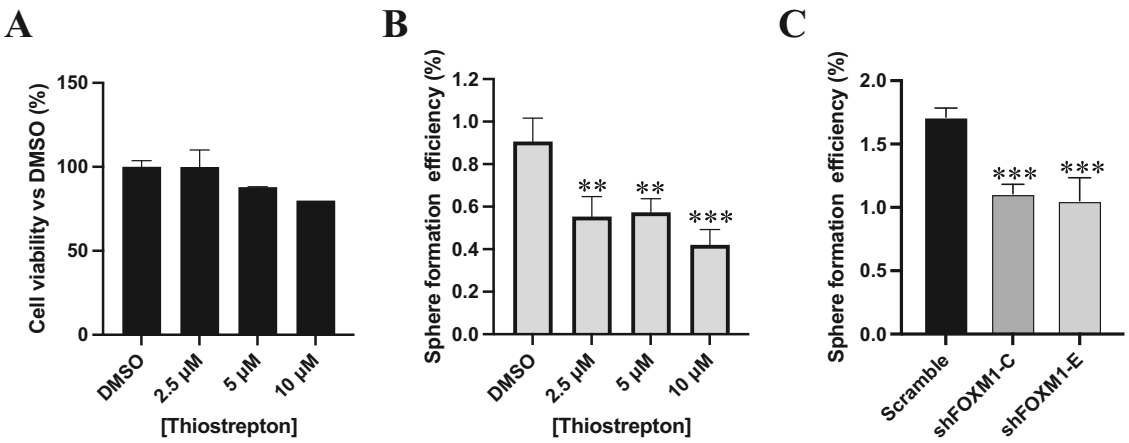

D

Group	Stem cell frequency (p=0.000267)
Scramble	1/99863
shFOXM1	1/466351

Fig. 3 FOXM1 sustains stemness in OC. A Viability of OC1 primary cells measured after 72 h of treatment with vehicle (DMSO) or 3 different doses of FOXM1 inhibitor Thiostrepton. **B** SFE in OC1 primary sample treated with vehicle (DMSO) or with 3 different doses of FOXM1 inhibitor Thiostrepton. Comparisons between experimental groups were done with two-sided Student's *t* test; $^{**}p < 0.01$, $^{***}p < 0.005$. **C** Sphere formation assay performed on TYK-nu cells expressing either a control shRNA (Scramble) or 2 different shRNAs against FOXM1 (shFOXM1-C and E). Comparisons between experimental groups were done with two-sided Student's *t* test; $^{***}p < 0.005$. **D** Nude mice were transplanted subcutaneously with decreasing numbers of either TYK-nu Scramble or TYK-nu shFOXM1-C cells, tumor take was assessed 21 days after injection (see Supplementary Fig. 3E) and an extreme limiting dilution assay (ELDA) was carried out to calculate the stem cell frequency ($p = 0.000267$).

TME/OCSC interplay in a clinically relevant setting, we have set up a platform of organotypic co-culture models, entirely built on patient-derived primary cells, which mimic the 3D architecture of the omental surface [9, 10]. Based on the architecture of the model and on the use of ascites-derived tumor cells, our approach recapitulates to a certain extent the initial contact between metastatic HGSOC cells present in the ascites and the omental niche during early peritoneal dissemination.

The first observation that derived from a global, unbiased transcriptome profiling of patient-derived organotypic co-cultures was that OCSC respond to the contact with peritoneal TME with the activation of pathways related to cell cycle, which is not observed in bulk cancer cells. This may be consistent with a pro-survival function of the TME which may underlie a (transient?) expansion of the OCSC pool and/or may trigger the initiation of the metastatic lesion of HGSOC.

In the transcriptome analysis, co-culture of OCSC with TME induced FOXM1 expression. Previously, this transcription factor was identified as part of a major network involved in the pathophysiology of HGSOC in the integrated multi-omics analysis of The Cancer Genome Atlas (TCGA) project [12]. Those findings, which support the ability of our organotypic approach to unveil pathways of clinical relevance, were subsequently confirmed and extended in several studies that implicated FOXM1 in HGSOC progression [13]. Nevertheless, our knowledge on the functional contribution of FOXM1 to OC stemness is scattered and derives from studies performed on cell lines with limited disease relevance [16, 18]. As an example of such limited relevance, TME-induced FOXM1 in OCSC, a phenomenon that was conserved across primary cultures from different patients, could be recapitulated only in TYK-nu cells among several cell lines. Furthermore, FOXM1 has never been analyzed in the context of OCSC/TME interactions. A previous study, in fact, has reported the role of FOXM1 on OC cell adhesion to mesothelium, yet without investigating specifically the CSC subpopulation [24]. By capitalizing on a fully patient-derived model, our study provides the first evidence of FOXM1 as a pivotal effector of TME-induced stemness features in HGSOC cells. As a corollary to our findings, such a mechanism may contribute to the regulatory role of the peritoneal niche on OCSC-driven dissemination, relapse and chemoresistance of HGSOC. In support of this paradigm, FOXM1 inhibition reduced peritoneal seeding in a syngeneic mouse model of OC [24] and sensitized OC cells to cisplatin and paclitaxel [34].

On the mechanistic level, organotypic co-cultures revealed that the induction of FOXM1 required the adhesion of OCSC to peritoneal TME and was mediated by FAK signaling. This is the first formal demonstration of a causal link between FAK activation and FOXM1 expression. The involvement of FAK in FOXM1-driven OC stemness is relevant given the many clinical trials that are assessing FAK inhibition in different tumor types including OC (https://clinicaltrials.gov/search?cond=ovariancancer&intr=Defactinib). Particularly intriguing, in this context, are the attempts to use FAK inhibition to re-sensitize OC to chemotherapy, which are being pursued also in the clinical setting (https://clinicaltrials.gov/study/NCT03287271) with the support of preclinical data implicating FAK activity in OC chemoresistance [35, 36]. Based on our findings, it is tempting to speculate that the ability of FAK inhibitors to restore chemosensitivity reflects, at least to a certain extent, the disruption of a FAK-FOXM1 axis that underlies OCSC-dependent drug resistance.

Our study clearly points to FOXM1 activity as a vulnerability in the pathophysiology of OCSC, implying that FOXM1-targeted treatments might offer a viable strategy to eradicate OC by eliminating its stem cell compartment. Despite its mechanism of action has not been fully clarified, Thiostrepton (also known as RSO-021) is the most widely used inhibitor of FOXM1, given its well-established ability to counteract this transcription factor, and

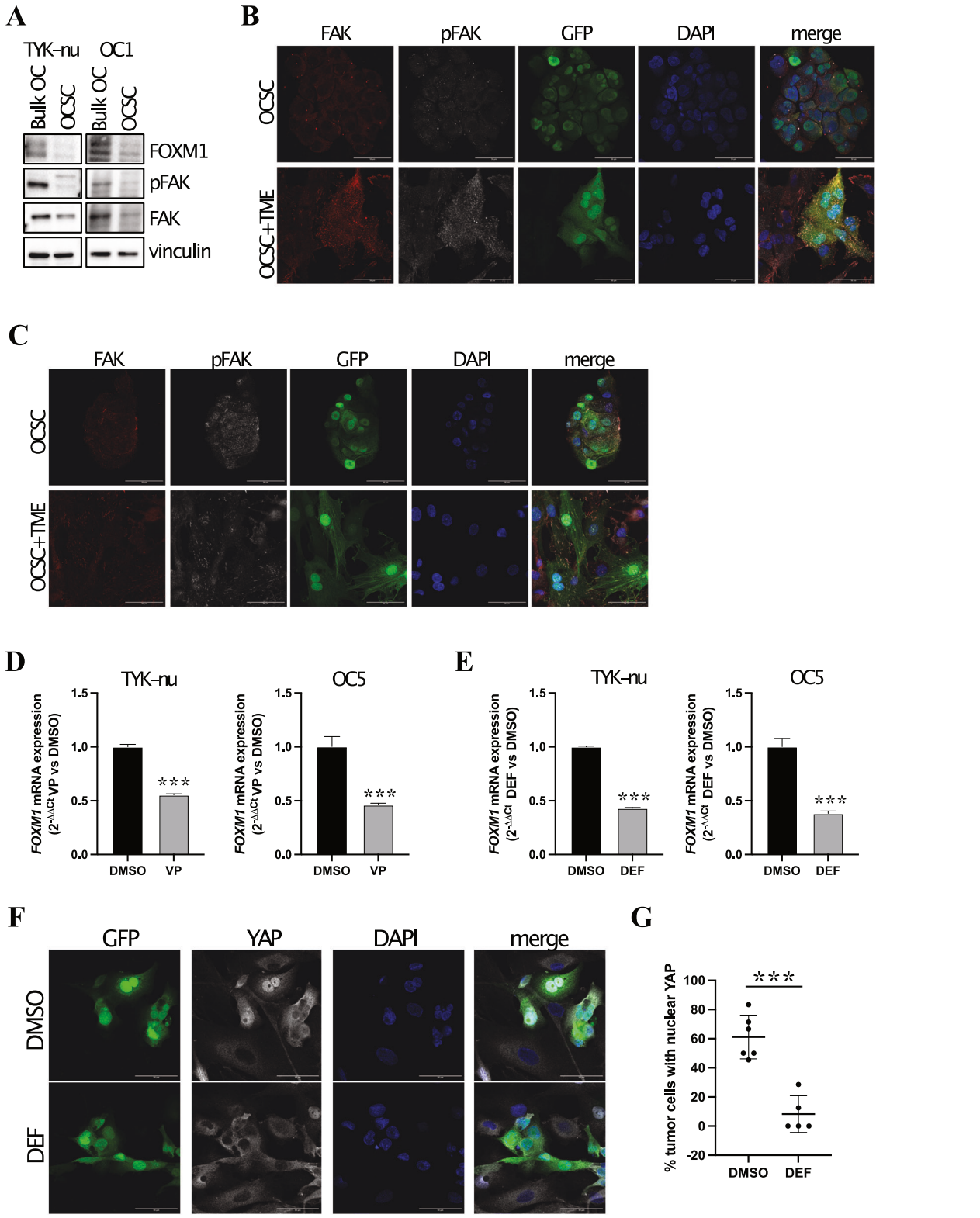

has been often used in mice showing no major toxicity [37–39]. Until recently, Thiostrepton has been used only in preclinical studies; however, a Phase I/II clinical trial in mesothelioma patients has recently started (https://clinicaltrials.gov/ct2/show/NCT05278975), which may prelude to the future use of Thiostrepton in the clinical practice and, hence, to its testing in OC patients.

In this context, we showed for the first time the increased efficacy of combining Thiostrepton and the PARPi Olaparib in reducing OCSC survival on TME. Based on these findings, we argue that the combination of FOXM1 inhibition and PARPi may prove an efficient therapeutic strategy for OC in the maintenance setting, due to its potential to synergistically interfere with OCSC-driven chemoresistance and tumor recurrence.

Fig. 4 Contact with TME induces FOXM1 signaling in OCSC through FAK/YAP signaling. A Cell lysates from TYK-nu and from primary sample OC1 cultured as bulk cells or OCSC were immunoblotted for FOXM1, pFAK and FAK, while vinculin was used as loading control. **B** Immunofluorescence for FAK (in red) and pFAK (in gray) on GFP^+ TYK-nu OCSC (in green) alone (upper panel) or co-cultured with TME (lower panel). Nuclei were counterstained with DAPI (blue). Scale bar: 50 μm. **C** Immunofluorescence for FAK (in red) and pFAK (in gray) on GFP^+ OCSC from primary sample OC1 (in green) alone (upper panels) or co-cultured with TME (lower panels). Nuclei were counterstained with DAPI (blue). Scale bar: 50 μm. **D** mRNA expression of *FOXM1* was analyzed by qRT-PCR in TYK-nu OCSC and in OCSC from primary sample OC5 cultured with TME for 24 h and treated with vehicle (DMSO, black) or with Verteporfin 3 μM (VP, gray). Data are represented as a relative mRNA expression ($2^{-\Delta\Delta Ct}$), compared to OCSC treated with DMSO. Comparisons between experimental groups were done with two-sided Student's *t* test; ***$p < 0.005$. **E** mRNA expression of *FOXM1* was analyzed by qRT-PCR in TYK-nu OCSC and in OCSC from primary sample OC5 cultured with TME for 24 h and treated with vehicle (DMSO, black) or with Defactinib 1 μM (DEF, gray). Data are represented as a relative mRNA expression ($2^{-\Delta\Delta Ct}$), compared to OCSC treated with DMSO. Comparisons between experimental groups were done with two-sided Student's *t* test; ***$p < 0.005$. **F** Immunofluorescence for YAP (in gray) on GFP^+ TYK-nu OCSC (in green) co-cultured with TME for 24 h and treated with vehicle (DMSO) or with Defactinib 1 μM (DEF). Nuclei were counterstained with DAPI (blue). Scale bar: 50 μm. **G** Quantification of the experiment shown in panel **E**. Each dot represents the percentage of OCSC positive for nuclear YAP signaling in a field. The graph shows mean ± SD of at least 5 fields. Comparisons between experimental groups were done with two-sided Student's *t* test; ***$p < 0.005$.

In summary, we have harnessed clinically relevant, patient-derived organotypic models to profile the impact of peritoneal TME to OCSC at the transcriptional level, which revealed FOXM1 as a novel, TME-induced driver of OCSC pathophysiology. Our data have profound implications not only for a deeper understanding of the pathogenic function of OCSC, but also as a starting point to develop innovative OCSC-eradicating therapies to defeat such a devastating tumor.

MATERIALS AND METHODS

Cell culture

The human ovarian cancer cell line TYK-nu was kindly provided by P. Lo Riso and G. Testa and was grown in MEM medium (Sigma-Aldrich, cat#G6148) containing 10% fetal bovine serum (FBS, Biowest cat# S1860), 2 mM L-glutamine (Euroclone, cat# ECB3000), 100 U/ml penicillin, 100 μg/ml streptomycin (Euroclone, cat# ECB3001). The cell line was routinely tested for mycoplasma with a PCR-based method and authenticated via short tandem repeat profiling.

Primary cell cultures were established from peritoneal ascites of high-grade serous ovarian cancer (HGSOC) patients. Tumor samples were provided by the Division of Gynecology at the European Institute of Oncology (Milan) upon informed consent from patients undergoing surgery. Clinicopathological features of the samples used in this work are provided in Supplementary Table S1. Tumor histology was confirmed by a board-certified pathologist (G. Bertalot), while the identity of cancer cells was confirmed by immunostaining for cytokeratins 5, 7, and 8, or for pan-cytokeratins. The purity of primary cell culture was consistently over 95%. Tissue isolation and culture conditions of primary cells were performed as described previously [40].

Mesothelial cells and fibroblasts were isolated from macroscopically healthy omental specimens, obtained upon informed consent from patients undergoing surgery for ovarian cancer at the European Institute of Oncology (Milan). To isolate mesothelial cells, the omental tissue was washed several times with sterile PBS, which was then collected and centrifuged at 1400 rpm for 5 min. Cell pellet containing mesothelial cells was cultured with RPMI 1640 (Euroclone, cat# ECM2001L), 20% FBS, 2 mM L-glutamine, 100 U/ml penicillin, 100 μg/ml streptomycin, 1% NEAA (Lonza, cat# 13-114E), 1% MEM vitamins (Lonza, cat# 13607C). To isolate fibroblasts, the tissue was minced and incubated overnight on an orbital shaker with 100 U of hyaluronidase (Merck, cat# H3884) and 1,000 U of collagenase type III (Worthington Biochemical, cat# LS004183) in DMEM (Euroclone, cat# ECM0103L), 10% FBS at 37 °C. The digested tissue was then centrifuged at 1400 rpm for 5 min, the cell pellet containing fibroblasts was washed with phosphate-buffered saline (PBS) and cultured in DMEM, 10% FBS, 1% glutamine, 100 U/ml penicillin, 100 μg/ml streptomycin, 1% NEAA, 1% MEM vitamins. Mesothelial cells and fibroblast were used for the experiments within three passages. Their identity was confirmed by immunostaining for WT1 and αSMA, which were specifically expressed by mesothelial cells and fibroblasts, respectively (Supplementary Fig. 1A, B).

All cell lines and primary samples were maintained at 37 °C in a humidified incubator with 5% CO_2.

When needed, cells were treated with the following reagents: Thiostrepton and Verteporfin from Sigma-Aldrich (cat# 598226 and SML0534, respectively); Defactinib and Olaparib from Selleckchem (cat# S7654 and S1060, respectively).

Sphere formation assay

Sphere formation assays were performed as described [41]. Briefly, single cell suspensions, derived from ovarian cancer cell lines or primary samples, were seeded at low density under non-adherent conditions in poly-(2-hydroxyethyl methacrylate)-coated dishes (Sigma-Aldrich, cat# P3932) and allowed to form clonal spheres. TYK-nu cells were seeded at a density of 5000 cells/ml, and OCSC-enriched sphere were maintained in DMEM:F-12 (1:1) (Gibco, cat# 11320033), supplemented with 2% B27 (Thermo Fisher Scientific, cat# 17504044;), 2 mM L-glutamine, 100 U/ml penicillin, 100 μg/ml streptomycin, 20 ng/mL epidermal growth factor (EGF, Merck, cat# E4127), and 10 ng/mL fibroblast growth factor-2 (FGF2; Peprotech, cat# AF-100-18B). Primary OCSC cultures were seeded at 5000 cells/ml in MEBM (Lonza, cat# CC-3151) supplemented with 2 mM L-glutamine, 100 U/mL penicillin, 100 μg/mL streptomycin, 5 μg/mL insulin (Thermo Fisher Scientific, cat# RP10935), 0.5 μg/mL hydrocortisone (Sigma-Aldrich, cat# H0888), 1 U/mL heparin (Voden, cat # 07980), 2% B27, 20 ng/mL EGF, and 20 ng/mL FGF2.

Spheres were then dissociated with StemPro Accutase (Thermo Fisher Scientific, cat# A1110501), according to the manufacturer's protocol, and re-plated under the same conditions to obtain second-generation spheres or used for co-cultures with the TME.

Sphere formation was assessed 5–10 days after seeding. The sphere-forming efficiency (SFE) was defined as the ratio between the number of spheres counted and the number of cells seeded.

Cell viability

Ovarian cancer cells were seeded in 96-well plates in quadruplicates at a density of 4000 cells/well, and after 24 h they were treated with different doses of Thiostrepton. After 72 h of treatment, the metabolic activity was quantified using the Cell counting kit-8 (Sigma-Aldrich, cat# 96992), following the manufacturer's instructions. The absorbance at a wavelength of 450 nm was measured using the Glomax Plate Reader.

For growth curves, TYK-nu cells were seeded in 96-well plates in quadruplicates at a density of 3000 cells/well, and then fixed and stained with crystal violet at each time point (0, 24, 48, 72, 96, 144 h). Crystal violet was then dissolved in 10% acetic acid and the absorbance at a wavelength of 590 nm was measured using the Glomax Plate Reader.

3D organotypic model

The 3D organotypic model was assembled as previously described [14]. Briefly, primary omental fibroblasts were resuspended in a medium containing 5 μg/ml collagen-I (Corning, cat# 354236) and 5 μg/ml fibronectin (Corning, cat# 354008), and then plated at a density of $6*10^3$ cells/cm^2 and incubated at 37 °C. After 4 h, the fibroblast layer was overlaid with primary mesothelial cells seeded at a density of $3*10^4$ cells/cm^2 and the co-culture was incubated at 37 °C for 2 days. Single-cell suspensions of OC cell lines or of primary HGSOC cells, pre-labeled with 0.1 μM CMFDA (Thermo Fisher Scientific, cat# C2925) according to manufacturer's instructions (in conditions that did not affect the viability of cancer cells), were seeded on top of 3D organotypic cultures, at the same density used for mesothelial cells. After 48 h, the co-cultures were dissociated to single cells and CMFDA-labeled HGSOC cells were isolated

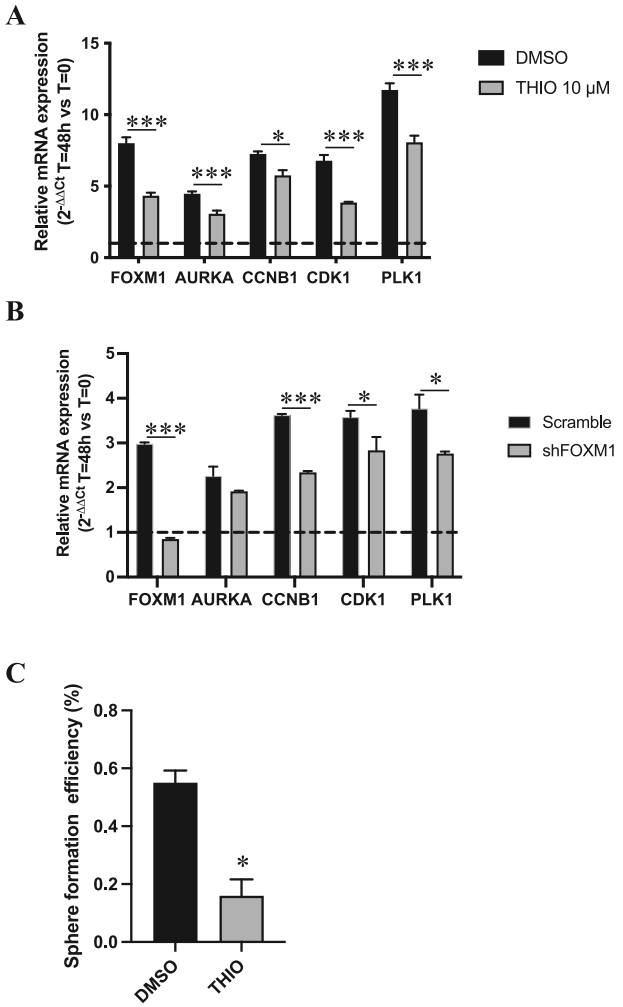

Fig. 5 TME stimulates the activation of FOXM1 pathway in OCSC. **A** mRNA expression of *FOXM1* and of its target genes (*AURKA*, *CCNB1*, *CDK1* and *PLK1*) was analyzed by qRT-PCR in OC1 OCSC cultured with TME for 48 h and treated with vehicle (DMSO, black) or with Thiostrepton 10 µM (gray). Data are represented as a relative mRNA expression ($2^{-\Delta\Delta Ct}$), compared to cells grown in absence of TME (dashed line). Comparisons between experimental groups were done with two-sided Student's *t* test; *$p < 0.05$, ***$p < 0.005$. **B** mRNA expression of *FOXM1* and of its target genes (*AURKA*, *CCNB1*, *CDK1* and *PLK1*) was analyzed by qRT-PCR in TYK-nu Scramble (black) or shFOXM1 (gray) OCSC cultured with TME for 48 h. Data are represented as a relative mRNA expression ($2^{-\Delta\Delta Ct}$), compared to Scramble OCSC not cultured with TME (dashed line). Comparisons between experimental groups were done with two-sided Student's *t* test; *$p < 0.05$, ***$p < 0.005$. **C** OC1 OCSC FACS-sorted after co-culture with TME in presence or absence of Thiostrepton 10 µM (experiment shown in panel **A**), were subjected to a sphere formation assay in absence of further treatments. Comparisons between experimental groups were done with two-sided Student's *t* test; *$p < 0.05$.

by fluorescence-activated cell sorting (FACS) and subjected to RNA extraction.

In some experiments, the 3D organotypic model was assembled in Nunc Lab-Tek chamber slides for immunofluorescence analysis, or in 96-well plates to assess response to drug treatments. In the latter case, GFP or RFP positive HGSOC cells were seeded on the TME, and after 24 h different drugs or drug combinations were added. Each treatment was performed in triplicate. After 5 days of treatment, nuclei were counterstained with Hoechst 33342 (Sigma-Aldrich, cat# 2261), and the fluorescent signal coming from GFP (or RFP) and Hoechst was acquired using the Leica THUNDER imaging system. Nine fields per well were acquired, and the area positive for GFP (or RFP) and Hoechst was quantified using the Fiji software. The GFP+ (or RFP+) area of treated cells was normalized on the one of vehicle-treated controls, to obtain the percentage of cells that survived at the end of treatment. For the drug combinations, the SinergyFinder web-tool (https://synergyfinder.fimm.fi/; [42]) was then used to quantify the degree of synergy, or antagonisms, of the tested combinations, using the Highest Single Agent (HSA) synergy scoring model. The resulting synergy scores were visualized as a 2D synergy map, which highlighted in red the drug concentrations displaying a synergistic effect, in green the ones with an antagonistic effect.

RNA extraction and qRT-PCR

Total RNA was extracted using the RNeasy Mini Kit (QIAGEN, cat# 217004) according to the manufacturer's protocol and quantified using the Nanodrop instrument (Thermo Fisher Scientific). RNA quality was checked using an Agilent 2100 Bioanalyzer. Preparation of cDNA and qRT-PCR were performed by the Cogentech qPCR Service (Milan, Italy).

Gene expression levels for *FOXM1* and its target genes were analyzed and normalized against the housekeeping genes *GAPDH* and *HPRT1*. TaqMan assays for specific genes are listed in Supplementary Table S5. Normalized expression changes were determined with the comparative threshold cycle ($2^{-\Delta\Delta CT}$) method.

RNA-Seq analysis

Poly-A enriched strand-specific libraries were generated with the TruSeq mRNA V2 sample preparation kit (Illumina, cat# RS-122-2001), ribosomal RNA depleted strand-specific RNA libraries with the TruSeq Stranded Total RNA LT sample preparation kit with Ribo-Zero Gold (Illumina, cat# RS-122-2301 and #RS-122-2302), and transcriptome capture based libraries with the TruSeq RNA Access Library Prep Kit (Illumina, cat# RS-301-2001). All protocols were performed following the manufacturer's instructions. Libraries were sequenced by Illumina NovaSeq 6000 resulting in paired 50nt reads. The sequencing coverage and quality statistics for each sample are summarized in Supplementary Table S6.

Fastq files were aligned to the hg38 genome assembly using STAR v 2.7.5c (PMID: 23104886). STAR gene counts were filtered by selecting those genes with raw counts > 10 in at least 2 out of 6 samples per each group of the comparison. Filtered gene counts were then normalized by the median of ratios method implemented in DESeq2 R package (PMID: 25516281). DESeq2 R package was used also to select differentially expressed genes between -TME (T0) and +TME (T48) in OCSC and bulk OC conditions. Heatmaps were generated by using Cluster 3.0 for Mac OS X (C Clustering Library 1.56) and Java TreeView version 1.1.6r4 (uncentered correlation and centroid linkage) using median centered $\log_2$ data.

Log_2FC data were subjected to Core Analysis of Ingenuity Pathway Analysis (IPA; QIAGEN) setting the following parameters: i) genes and endogenous chemical as Reference Set; ii) direct and indirect relationship; iii) human as Species. Canonical Pathways and Upstream Regulators results of the Core Analysis were considered.

Gene Set Enrichment Analysis (GSEA; https://www.gsea-msigdb.org/gsea/index.jsp; PMID: 12808457 and 16199517) was performed using the "xtools.gsea.GseaPreranked" tool to input expression data ordered by the "Stat" output of DESeq2 R package (i.e., Wald statistic) in the case of TME in OCSC condition. In the case of TCGA-OC dataset, GSEA was performed by correlating expression data to FOXM1 expression profile by Pearson correlation metric. One-thousand random gene sets permutation was performed for false discovery rate (FDR) computation of the normalized enrichment scores (NES). Hallmark gene sets ($N = 50$) (https://www.gsea-msigdb.org/gsea/msigdb/human/collections.jsp) or specific gene sets representative of YAP signaling (CORDENONSI_YAP_CONSERVED_SIGNATURE.v2022.1.Hs.gmt) and FOXM1 transcription factor network (PID_FOXM1_PATHWAY.v7.5.1.gmt.txt) were used.

Single cell preparation, cDNA synthesis, generation of single cell GEM and libraries construction

The single cell library was performed according to the manufacture protocol "Chromium Next GEM Single Cell 3' Reagent Kits v3.1 (dual Index). Briefly, the chromium single cell gene expression workflow requires around 8 h and it's splitable in 3 different steps: the GEM generation, the cDNA amplification and the library construction. The first step is performed by 10X Genomics Chromium Controller instrument loading cells, enzyme, beads and oil into the microfluidics chip. The emulsion produces thousands of cells into nanoliter-scale drop of oil named gel bead-in-

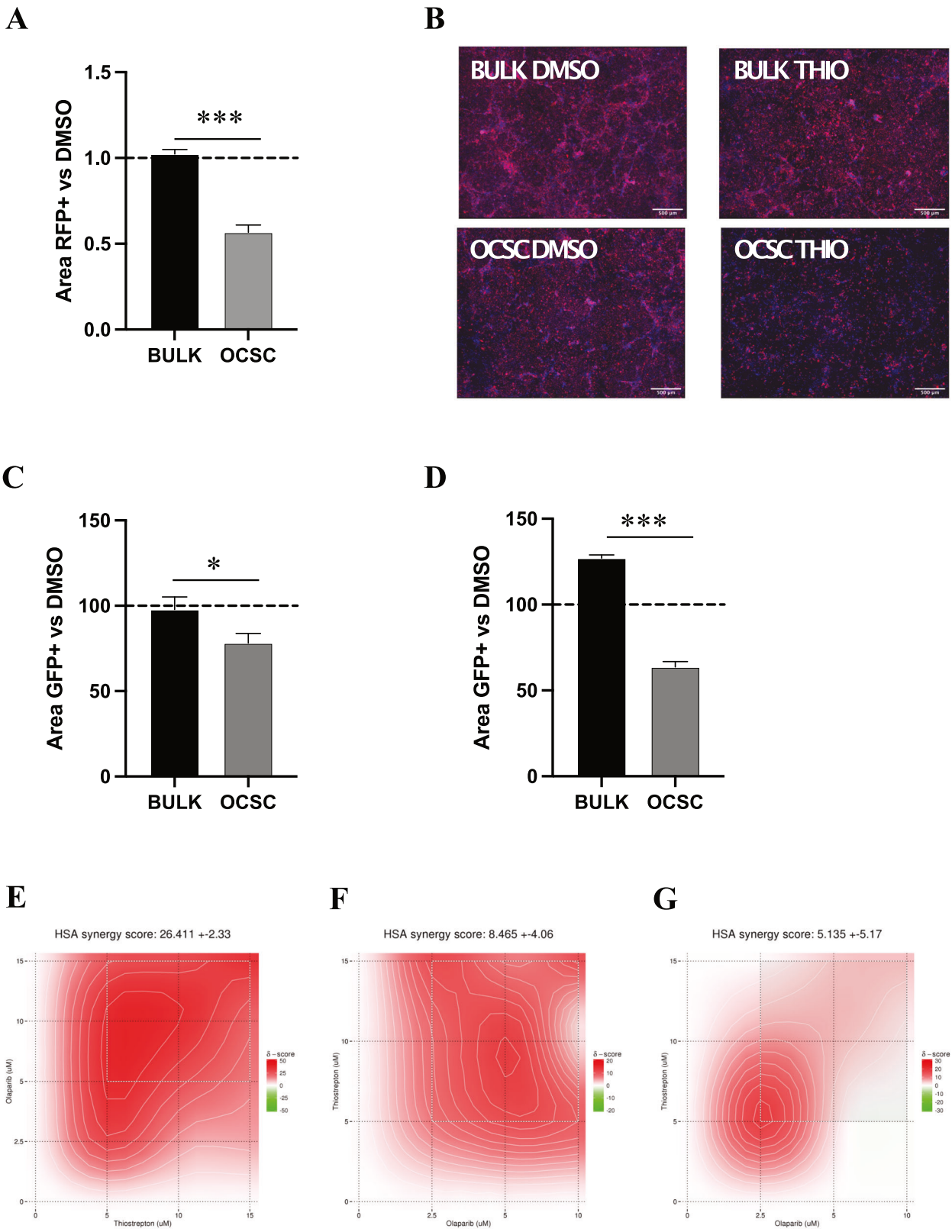

emulsions (GEMs). To achieve single cell resolution, the cells are delivered at a limiting dilution, such that the majority (~90–99%) of generated gems contains no cell; while the remaining gems contain a single cell. The primers coated on the beads, containing, Illumina R1 sequence, 10x barcode, UMI, and Poly dt, are mixed with cell lysis buffer and master mix. Incubation of the gems then produce barcoded full-length cDNA from poly adenylated RNA. The full-length, barcoded cDNA is amplified by PCR to generate sufficient mass for the Illumina library construction. At the end of the library generation, we obtain a standard Illumina paired-end library with this follow structure: P5 and P7 used for the Illumina bridge amplification, two sequencing primers annealing region, 16 bp 10x barcode for the cell identification, 12 bp UMI to count the transcripts,

Fig. 6 FOXM1 inhibition decreases survival of OCSC cultured on TME and synergizes with PARP inhibitors. A RFP positive TYK-nu bulk and OCSC were cultured on TME in presence of Thiostrepton 10 μM, and RFP positive area was measured after 6 days of treatment. Data are expressed as mean RFP^+ area ±SEM from 3 independent experiments. Comparisons between experimental groups were done with two-sided Student's *t* test; ***$p < 0.005$. **B** Representative pictures from one of the experiments analyzed in panel **A**. Scale bar: 500 μm. GFP positive bulk and OCSC from primary samples OC6 (**C**) and OC10 (**D**) were cultured on TME in the presence of 10 μM Thiostrepton, and GFP positive area was measured after 6 days of treatment. Data are expressed as mean GFP^+ area ±SD from one representative experiment ($n = 3$). Comparisons between experimental groups were done with two-sided Student's *t* test; *$p < 0.05$, ***$p < 0.005$. **E** RFP positive TYK-nu OCSC were cultured on TME and treated with 3 different doses of Thiostrepton (5, 10 and 15 μM) and 4 doses of Olaparib (2.5, 5, 10 and 15 μM), alone or in combination. RFP positive area was measured after 6 days of treatment. The combinatorial matrix shows the synergy distribution for the drug combinations according to the Gaddum's non-interaction (HSA) model, calculated using the SynergyFinder Web Application. The intensity of red color reflects the strength of synergism of each drug concentration. The panel shows the result of one representative experiment ($n = 3$). GFP positive OCSC from OC9 (**F**) and OC10 (**G**) primary sample were cultured on TME and treated with 3 different doses of Thiostrepton (5, 10 and 15 μM) and 3 doses of Olaparib (2.5, 5 and 10 μM), alone or in combination. GFP positive area was measured after 6 days of treatment. The combinatorial matrix shows the synergism distribution for the drug combinations according to the Gaddum's non-interaction (HSA) model, calculated using the SynergyFinder Web Application.

cDNA from the 3'utr region of the gene and two sample indexes to demultiplex the pool of samples loaded on the sequencer.

Amplified libraries are checked on a bioanalyzer 2100 and quantified with picogreen reagent. Libraries with distinct indexes are multiplexed and after cluster generation on Flow Cell are sequenced for 28-10-10-90 bases in the paired-end mode with 5×10^4 reads per cell in coverage on a Novaseq 6000 sequencer.

Single cell analysis

Identification of contaminant normal omentum cells. To exclude normal omental cells possibly escaping FACS selection, we used a method [43] based on the call of mutations from sample-matched bulk RNAseq data, that are next used to demultiplex single cell data. Briefly, we generated variant calling files (VCF) from bulk RNAseq data derived from tumor and normal omental cells prior to co-colture. In parallel, single cell RNAseq data were aligned using cellranger 4.0.0 using the reference provided by 10x genomics. The VCF files and the single cell data were used to define doublet cells and demultiplexing through the application of three methods, i.e. Vireo [44], Demuxlet [45] and SCanSNP [43], whose aggregated score (Consensus) was used to filter out cells derived from normal omental cells and doublets as described in Ref. [43].

Single cell data preparation. All downstream analyses were performed within scanpy single cell analysis framework [46]. Basic filtering was performed after importing count matrices from cellranger 4.0.0. We inspected the number of genes and mitochondrial gene counts distributions and adopted thresholds to remove droplets with likely technical issues. Cell counts were normalized, log transformed using *sc.pp.normalize_total* and *sc.pp.log1p* scanpy functions. Finally we regressed out the effect of total counts and the percentage of mitochondrial transcripts via *sc.pp.regress_out* and *sc.pp.scale* functions. All functions were run with default parameters.

Highly variable genes (HVGs) selection. We detected HVGs via *sc.pp.highly_variable_genes* scanpy function, providing each dataset as a separate batch and *min_mean* = 0.0125, *max_mean* = 3, *min_disp* = 0.5 as parameters.

Dimensionality reduction and datasets' integration. After final dataset cleaning we computed PCA in HVGs, the subsequent datasets' integration was carried out via scanpy's BBKNN implementation [47] with default parameters.

Cell cycle inference. To impute the cell cycle phase for each cell (G1, S, G2M), we used the scanpy implementation of a previously described method [48], using the function *sc.tl.score_genes_cell_cycle*, which assigns to each cell a score for each cell cycle phase based on the expression of phase-specific genes.

FOXM1 analysis. To characterize the expression of the FOXM1 gene, we restricted our analysis to FOXM1 positive cells, defined as having a normalized scaled level of expression > 0. Among positive cells, we derived the distribution of expression of this gene in different cell cycle phases among the considered conditions (cell cycle phases, sample type, patients) and visualized them through violin plots.

Immunoblotting

Cells were lysed in hot lysis buffer (2.5% SDS, 125 mM Tris-HCl [pH 6.8]), after 15 min incubation at 95 °C.

For cytosolic/nuclear fractionation, cells were washed with ice-cold PBS and incubated with a hypotonic buffer (10 mM Hepes pH 7.9, 10 mM KCl, 0.1 mM EDTA, 0.1 mM EGTA, 0.6% NP-40, 1 mM $NaVO_3$, 1:500 Protease Inhibitors Cocktail from Sigma-Aldrich cat# P8340) for 20 min on ice in a shaker. Cells were then scraped and collected in an eppendorf tube. After centrifugation for 10 min at maximum speed, the supernatant containing the cytoplasmic fraction was collected. For nuclear extracts, the pellet was washed 3 times with the same buffer and then incubated with the nuclear lysis buffer (20 mM Hepes pH 7.9, 400 mM NaCl, 0.1 mM EDTA, 0.1 mM EGTA, 50% Glycerol, 1 mM $NaVO_3$, 1:500 Protease Inhibitors Cocktail) for 1 h in a shaker at 4 °C. After centrifugation for 5 min at maximum speed, the supernatant containing the nuclear fraction was collected.

Protein concentration was determined using a Pierce BCA Protein Assay kit (Thermo Fisher Scientific, Inc, cat# 23227) according to the manufacturer's instructions. Equal amounts of protein extracts (20 μg) were resolved in acrylamide gel and transferred onto nitrocellulose membranes. The membranes were incubated overnight at 4 °C with the following primary antibodies: FOXM1 (Cell Signaling, cat# 5436), FAK (Invitrogen, cat# 39-6500), phospho-FAK (Tyr397) (Invitrogen, cat# 700255), YAP (Cell Signaling, cat# 14074), beta-Tubulin (Santa Cruz, cat# sc-58886), vinculin (Sigma-Aldrich, cat# V9131), Lamin A/C (Santa Cruz, cat# sc-7292). Membranes were incubated with IgG HRP-conjugated secondary antibody (Bio-Rad Laboratories) for 1 h at room temperature. The signal was detected by the Clarity Western ECL Substrate (Bio-Rad, cat# 1705062) as described in the manufacturers protocol and the images were acquired using ChemiDoc (Bio-Rad) and analyzed with the Fiji software.

Immunofluorescence

Cultured cells (or cytospins with OCSC-enriched spheres) were fixed with 4% paraformaldehyde for 5 min at room temperature and then permeabilized in ice-cold PBS, 0.5% Triton X-100 for 3 min at 4 °C. After blocking for 1 h at room temperature with blocking buffer (PBS, 0.2% BSA, 1% donkey serum, 0.05% Tween-20 and 0.02% NaN3), cells were incubated for 2 h with the following primary antibodies, diluted in blocking buffer: FOXM1 (Cell Signaling, cat# 5436), FAK (Invitrogen, cat# 39-6500), phospho-FAK (Tyr397) (Invitrogen, cat# 700255), YAP (Cell Signaling, cat# 14074), WT1 (Abcam, cat# ab89901), αSMA (Abcam, cat# ab7817). Cells were then washed with PBS and incubated with the Alexa Fluor-conjugated secondary antibodies (Jackson Laboratories) for 1 h at room temperature. Nuclei were counterstained with DAPI (Sigma-Aldrich, cat# 32670). Images were acquired using the Leica SP8 Confocal microscope.

Lentivirus production and cell transduction

Lentiviral vectors were generated by transient co-transfection of the packaging cell line HEK293T, purchased from ATCC and cultured as described previously [40], with 10 μg of the following anti-FOXM1 shRNA from Genecopoeia: sh-C (5'-TAATACGACTCACTATAGGG-3'; HSH096566-LVRU6GP-c); sh-E (5'-TAATACGACTCACTATAGGG-3'; HSH096566-LVRU6GP-e) or with the scrambled control (CSHCTR001-LVRU6GP, Genecopoeia), and the following packaging vectors: PMD2G (3 μg), Rre (5 μg), and REV (2.5 μg), using the calcium phosphate precipitation method. The supernatant from HEK293T, containing the virus particles, was supplemented with 8 μg/ml of polybrene and used to transduce recipient cells.

In vivo limiting dilution assays

Mice were housed under specific pathogen-free conditions in isolated vented cages and allowed access to food and water ad libitum. Six-eight weeks-old nude female mice (from Charles River Laboratories) were injected subcutaneously into the flank with serial dilutions of TYK-nu shSCR and shFOXM1 cells, ranging between $5*10^6$ and $1*10^4$ cells/site in a 1:1 (vol:vol) mixture with growth factor-reduced Matrigel (Corning, cat# 356231) and PBS, with a final volume of 100 µl per injection. Each experimental group consisted of 7 mice.

Tumor latency was defined as the time interval from the injection to the formation of palpable tumors. Tumor take frequency was determined as the number of mice with palpable tumors. Cancer stem cell frequency was measured using the ELDA online software http://bioinf.wehi.edu.au/software/elda.

Body weight and general physical status were monitored daily, and the mice were sacrificed when the tumor reached a volume of 1000 mm^3.

All experimental procedures involving mice and their care were performed following protocols approved by the fully authorized animal facility of our Institutions and by the Italian Ministry of Health (as required by the Italian Law) (protocol no. 239/2023-PR) and in accordance with EU directive 2010/63.

Statistical analysis

Independent experiments were considered as biological replicates. For in vivo experiments, each mouse represented one biological replicate. Data are expressed as means ± SEM, calculated from at least three independent experiments. Statistical significance was evaluated with Student's two-tailed *t* test (GraphPad Prism 8). Cut-off threshold to define significance was set at $p < 0.05$. Asterisks correspond to the *p*-value calculated by a two-tailed, unpaired t-test (*$p < 0.05$, **$p < 0.01$, ***$p < 0.001$).

DATA AVAILABILITY

The transcriptomic data generated in this study have been deposited in the European Genome-Phenome Archive (EGA) under the following accession codes: Study EGAS50000000355; Dataset EGAD50000000523. The data are available under restricted access in accordance with art. 13 General Regulation on Data Protection (EU Regulation 2016/679); access can be obtained by request to EGA and approval by the competent Data Access Committee. Please contact the corresponding author for access requests. The TCGA Ovarian Serous Cystadenocarcinoma (OV) RMA normalized dataset (samples with mRNA data, U133 microarray data only, N = 535) was downloaded from GDAC firehose through cBioPortal data portal (https://www.cbioportal.org/study/summary?id=ov_tcga).

REFERENCES

1. Marchetti C, De Felice F, Romito A, Iacobelli V, Sassu CM, Corrado G, et al. Chemotherapy resistance in epithelial ovarian cancer: Mechanisms and emerging treatments. Semin Cancer Biol. 2021;77:144–66.
2. Bray F, Ferlay J, Soerjomataram I, Siegel RL, Torre LA, Jemal A. Global cancer statistics 2018: GLOBOCAN estimates of incidence and mortality worldwide for 36 cancers in 185 countries. CA Cancer J Clin. 2018;68:394–424.
3. Ritch SJ, Telleria CM. The Transcoelomic Ecosystem and Epithelial Ovarian Cancer Dissemination. Front Endocrinol. 2022;13:886533.
4. Lupia M, Cavallaro U. Ovarian cancer stem cells: Still an elusive entity? Mol Cancer. 2017;16:64.
5. Nwani NG, Sima LE, Nieves-Neira W, Matei D. Targeting the Microenvironment in High Grade Serous Ovarian Cancer. Cancers (Basel). 2018;10:266.
6. Cummings M, Freer C, Orsi NM. Targeting the tumour microenvironment in platinum-resistant ovarian cancer. Semin cancer Biol. 2021;77:3–28.
7. Lengyel E. Ovarian cancer development and metastasis. Am J Pathol. 2010;177:1053–64.
8. Kenny HA, Lal-Nag M, Shen M, Kara B, Nahotko DA, Wroblewski K, et al. Quantitative High-Throughput Screening Using an Organotypic Model Identifies Compounds that Inhibit Ovarian Cancer Metastasis. Mol Cancer Ther. 2020;19:52–62.
9. Kenny HA, Kaur S, Coussens LM, Lengyel E. The initial steps of ovarian cancer cell metastasis are mediated by MMP-2 cleavage of vitronectin and fibronectin. J Clin invest. 2008;118:1367–79.
10. Kenny HA, Chiang C-Y, White EA, Schryver EM, Habis M, Romero IL, et al. Mesothelial cells promote early ovarian cancer metastasis through fibronectin secretion. J Clin invest. 2014;124:4614–28.
11. Hart PC, Kenny HA, Grassl N, Watters KM, Litchfield LM, Coscia F, et al. Mesothelial Cell HIF1a Expression Is Metabolically Downregulated by Metformin to Prevent Oncogenic Tumor-Stromal Crosstalk. Cell Rep. 2019;29:4086–98.e6.
12. Cancer Genome Atlas Research N. Integrated genomic analyses of ovarian carcinoma. Nature. 2011;474:609–15.
13. Liu C, Barger CJ, Karpf AR. FOXM1: A Multifunctional Oncoprotein and Emerging Therapeutic Target in Ovarian Cancer. Cancers. 2021;13:3065.
14. Kenny HA, Krausz T, Yamada SD, Lengyel E. Use of a novel 3D culture model to elucidate the role of mesothelial cells, fibroblasts and extra-cellular matrices on adhesion and invasion of ovarian cancer cells to the omentum. Int J Cancer. 2007;121:1463–72.
15. Raychaudhuri P, Park HJ. FOXM1: a master regulator of tumor metastasis. Cancer Res. 2011;71:4329–33.
16. Ning YX, Li QX, Ren KQ, Quan MF, Cao JG. 7-difluoromethoxyl-5,4′-di-n-octyl genistein inhibits ovarian cancer stem cell characteristics through the down-regulation of FOXM1. Oncol Lett. 2014;8:295–300.
17. Chiu W-T, Huang Y-F, Tsai H-Y, Chen C-C, Chang C-H, Huang S-C, et al. FOXM1 confers to epithelial-mesenchymal transition, stemness and chemoresistance in epithelial ovarian carcinoma cells. Oncotarget. 2014;6:2349–65.
18. Young MJ, Wu YH, Chiu WT, Weng TY, Huang YF, Chou CY. All-trans retinoic acid downregulates ALDH1-mediated stemness and inhibits tumour formation in ovarian cancer cells. Carcinogenesis. 2015;36:498–507.
19. Kwok JMM, Myatt SS, Marson CM, Coombes RC, Constantinidou D, Lam EWF. Thiostrepton selectively targets breast cancer cells through inhibition of forkhead box M1 expression. Mol Cancer Therapeutics. 2008;7:2022–32.
20. Ince TA, Sousa AD, Jones MA, Harrell JC, Agoston ES, Krohn M, et al. Characterization of twenty-five ovarian tumour cell lines that phenocopy primary tumours. Nat Commun. 2015;6:7419.
21. Domcke S, Sinha R, Levine DA, Sander C, Schultz N. Evaluating cell lines as tumour models by comparison of genomic profiles. Nat Commun. 2013;4:2126.
22. Hu Y, Smyth GK. ELDA: Extreme limiting dilution analysis for comparing depleted and enriched populations in stem cell and other assays. J Immunol Meth. 2009;347:70–8.
23. Cooper J, Giancotti FG. Integrin Signaling in Cancer: Mechanotransduction, Stemness, Epithelial Plasticity, and Therapeutic Resistance. Cancer Cell. 2019;35:347–67.
24. Parashar D, Nair B, Geethadevi A, George J, Nair A, Tsaih SW, et al. Peritoneal spread of ovarian cancer harbors therapeutic vulnerabilities regulated by FOXM1 and EGFR/ERBB2 signaling. Cancer Res. 2020;80:5554–68.
25. Rausch V, Hansen CG. The Hippo Pathway, YAP/TAZ, and the Plasma Membrane. Trends Cell Biol. 2020;30:32–48.
26. Mizuno T, Murakami H, Fujii M, Ishiguro F, Tanaka I, Kondo Y, et al. YAP induces malignant mesothelioma cell proliferation by upregulating transcription of cell cycle-promoting genes. Oncogene. 2012;31:5117–22.
27. Fan Q, Cai Q, Xu Y. FOXM1 is a downstream target of LPA and YAP oncogenic signaling pathways in high grade serous ovarian cancer. Oncotarget. 2015;6:27688–99.
28. Moore K, Colombo N, Scambia G, Kim B-G, Oaknin A, Friedlander M, et al. Maintenance Olaparib in Patients with Newly Diagnosed Advanced Ovarian Cancer. N Engl J Med. 2018;379:2495–505.
29. González-Martín A, Pothuri B, Vergote I, DePont Christensen R, Graybill W, Mirza MR, et al. Niraparib in Patients with Newly Diagnosed Advanced Ovarian Cancer. N Engl J Med. 2019;381:2391–402.
30. Ray-Coquard I, Pautier P, Pignata S, Pérol D, González-Martín A, Berger R, et al. Olaparib plus Bevacizumab as First-Line Maintenance in Ovarian Cancer. N Engl J Med. 2019;381:2416–28.
31. Wu SQ, Huang SH, Lin QW, Tang YX, Huang L, Xu YG, et al. FDI-6 and olaparib synergistically inhibit the growth of pancreatic cancer by repressing BUB1, BRCA1 and CDC25A signaling pathways. Pharm Res. 2022;175:106040.
32. Wang SP, Wu SQ, Huang SH, Tang YX, Meng LQ, Liu F, et al. FDI-6 inhibits the expression and function of FOXM1 to sensitize BRCA-proficient triple-negative breast cancer cells to Olaparib by regulating cell cycle progression and DNA damage repair. Cell Death Dis. 2021;12:1–12.
33. Munoz-Galvan S, Carnero A. Targeting Cancer Stem Cells to Overcome Therapy Resistance in Ovarian Cancer. Cells. 2020;9:1402.
34. Westhoff GL, Chen Y, Teng NNH. Targeting FOXM1 Improves Cytotoxicity of Paclitaxel and Cisplatinum in Platinum-Resistant Ovarian Cancer. Int J Gynecologic Cancer. 2017;27:1602–9.
35. Levy A, Alhazzani K, Dondapati P, Alaseem A, Cheema K, Thallapureddy K, et al. Focal Adhesion Kinase in Ovarian Cancer: A Potential Therapeutic Target for Platinum and Taxane-Resistant Tumors. Curr Cancer Drug Targets. 2019;19:179–88.
36. Diaz Osterman CJ, Ozmadenci D, Kleinschmidt EG, Taylor KN, Barrie AM, Jiang S, et al. FAK activity sustains intrinsic and acquired ovarian cancer resistance to platinum chemotherapy. Elife. 2019;8:e47327.
37. Zhang W, Gong M, Zhang W, Mo J, Zhang S, Zhu Z, et al. Thiostrepton induces ferroptosis in pancreatic cancer cells through STAT3/GPX4 signalling. Cell Death Dis. 2022;13:630.

38. Siraj AK, Pratheeshkumar P, Parvathareddy SK, Qadri Z, Thangavel S, Ahmed S, et al. FoxM1 is an independent poor prognostic marker and therapeutic target for advanced Middle Eastern breast cancer. Oncotarget. 2018;9:17466–82.
39. Pratheeshkumar P, Divya SP, Parvathareddy SK, Alhoshani NM, Al-Badawi IA, Tulbah A, et al. FoxM1 and beta-catenin predicts aggressiveness in Middle Eastern ovarian cancer and their co-targeting impairs the growth of ovarian cancer cells. Oncotarget. 2018;9:3590–604.
40. Francavilla C, Lupia M, Tsafou K, Villa A, Kowalczyk K, Rakownikow Jersie-Christensen R, et al. Phosphoproteomics of Primary Cells Reveals Druggable Kinase Signatures in Ovarian Cancer. Cell Rep. 2017;18:3242–56.
41. Lupia M, Angiolini F, Bertalot G, Freddi S, Sachsenmeier KF, Chisci E, et al. CD73 Regulates Stemness and Epithelial-Mesenchymal Transition in Ovarian Cancer-Initiating Cells. Stem Cell Rep. 2018;10:1412–25.
42. Zheng S, Wang W, Aldahdooh J, Malyutina A, Shadbahr T, Tanoli Z, et al. SynergyFinder Plus: Toward Better Interpretation and Annotation of Drug Combination Screening Datasets. Genomics Proteom Bioinforma. 2022;20:587–96.
43. Nicolò C, Davide C, Marco Tullio R, Cristina C, Sebastiano T, Alessia V, et al. Multiplexing cortical brain organoids for the longitudinal dissection of developmental traits at single cell resolution. bioRxiv. 2023. https://www.biorxiv.org/content/10.1101/2023.08.21.553507v1.
44. Huang Y, McCarthy DJ, Stegle O. Vireo: Bayesian demultiplexing of pooled single-cell RNA-seq data without genotype reference. Genome Biol. 2019;20:273.
45. Kang HM, Subramaniam M, Targ S, Nguyen M, Maliskova L, McCarthy E, et al. Multiplexed droplet single-cell RNA-sequencing using natural genetic variation. Nat Biotechnol. 2018;36:89–94.
46. Wolf FA, Angerer P, Theis FJ. SCANPY: large-scale single-cell gene expression data analysis. Genome Biol. 2018;19:15.
47. Polański K, Young MD, Miao Z, Meyer KB, Teichmann SA, Park JE. BBKNN: fast batch alignment of single cell transcriptomes. Bioinformatics. 2020;36:964–5.
48. Kowalczyk MS, Tirosh I, Heckl D, Rao TN, Dixit A, Haas BJ, et al. Single-cell RNA-seq reveals changes in cell cycle and differentiation programs upon aging of hematopoietic stem cells. Genome Res. 2015;25:1860–72.

ACKNOWLEDGEMENTS

We are grateful to all patients who donated their samples for this work, to the Ovarian Cancer Center staff at IEO (Milano) for providing the tumor samples, and to the IEO Biobank staff for collection and annotation of surgical samples. We thank F. Balkwill and B. Malacrida for helpful discussion; G. Bertalot for the histological analysis of tumor specimens; the staff of the Units of Genomics, Cell Culture and FACS at IEO; and D. Capocefalo and M. Sallese for the support in the analysis of scRNAseq. This work was supported by grants from Ovarian Cancer Research Alliance (Collaborative Research Development Grant 648516 to UC, EL), Associazione Italiana Ricerca sul Cancro (IG-21320 to UC; IG-22827 to FB; IG-23250 to RG), the Italian Ministry of Health (PE-2016-02362551 to UC; RF-2021-12372433 to FB). The study funders had no role in the study's design, collection, analysis, and interpretation of the data, writing of the manuscript, and the decision to submit the manuscript for publication. Fabrizio Bianchi wishes to dedicate this work to the memory of Lucia, an extraordinary girl who experienced cancer as an opportunity to entrust her and all her loved ones to the love of the Father.

AUTHOR CONTRIBUTIONS

CB acquired and interpreted data, and drafted the manuscript; HAK, AD, acquired data and revised the manuscript; MZ, VN, AG acquired data; MG and FMP provided samples; VM, PLR, CEV performed bioinformatics analyses; GT, RG, NC, FB, EL contributed to data interpretation, supervised some of the work and revised the manuscript; UC conceived and supervised the work, interpreted data, and drafted the manuscript. All authors read and approved the final manuscript.

COMPETING INTERESTS

The authors declare no competing interests.

ETHICS APPROVAL AND CONSENT TO PARTICIPATE

This study was conducted in compliance with the principles of the Declaration of Helsinki. Informed consent was obtained from all the subjects. Sample collection was performed under the protocol no. R789-IEO approved by the Ethics Committee of the European Institute of Oncology.

ADDITIONAL INFORMATION

Supplementary information The online version contains supplementary material available at https://doi.org/10.1038/s41419-024-06767-7.

Correspondence and requests for materials should be addressed to Ugo Cavallaro.

Reprints and permission information is available at http://www.nature.com/reprints

Publisher's note Springer Nature remains neutral with regard to jurisdictional claims in published maps and institutional affiliations.